






Ni(II) and Cu(II) complexes of new unsymmetrical N₂O₂ Schiff bases derived from 3-(2-aminobenzylimino)-1-phenylbutan-1-ol: synthesis, structure, antibacterial properties, and electrochemistry

Soraia Meghdadi, Mehdi Amirnasr, Kurt Mereiter, Somayeh Motaharipour, Monireh Nasehi, Maryam Bagheri & Soheila Abbasi


To cite this article: Soraia Meghdadi, Mehdi Amirnasr, Kurt Mereiter, Somayeh Motaharipour, Monireh Nasehi, Maryam Bagheri & Soheila Abbasi (2015) Ni(II) and Cu(II) complexes of new unsymmetrical N₂O₂ Schiff bases derived from 3-(2-aminobenzylimino)-1-phenylbutan-1-ol: synthesis, structure, antibacterial properties, and electrochemistry, Journal of Coordination Chemistry, 68:22, 4055-4069, DOI: [10.1080/00958972.2015.1085977](https://doi.org/10.1080/00958972.2015.1085977)


To link to this article: <http://dx.doi.org/10.1080/00958972.2015.1085977>

 View supplementary material 

 Accepted author version posted online: 26 Aug 2015.
Published online: 16 Sep 2015.

 Submit your article to this journal 

 Article views: 97

 View related articles 

 View Crossmark data 

Ni(II) and Cu(II) complexes of new unsymmetrical N₂O₂ Schiff bases derived from 3-(2-aminobenzylimino)-1-phenylbutan-1-ol: synthesis, structure, antibacterial properties, and electrochemistry

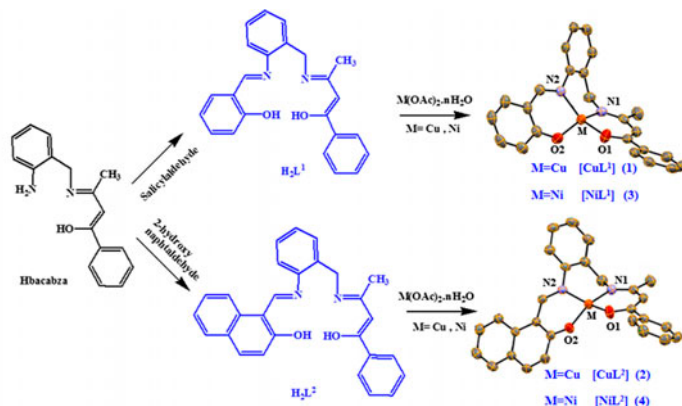
SORAIA MEGHDADI[†], MEHDI AMIRNASR^{*†}, KURT MEREITER[‡],
SOMAYEH MOTAHARIPOUR[†], MONIREH NASEHI[†], MARYAM BAGHERI[†] and
SOHEILA ABBASI[§]

[†]Department of Chemistry, Isfahan University of Technology, Isfahan, Iran

[‡]Faculty of Chemistry, Vienna University of Technology, Vienna, Austria

[§]Department of Biological Sciences, University of Isfahan, Isfahan, Iran

(Received 26 October 2014; accepted 30 July 2015)



Two new N₂O₂ unsymmetrical Schiff bases, H₂L¹ = 3-[(*o*-[(*E*)-(2-hydroxyphenyl)methylideneamino]phenyl)methyl]imino]-1-phenyl-1-buten-1-ol and H₂L² = 3-[(*o*-[(*E*)-(2-hydroxy-1-naphthyl)methylideneamino]phenyl)methyl]imino]-1-phenyl-1-buten-1-ol, and their copper(II) and nickel(II) complexes, [CuL¹] (1), [CuL²] (2), [NiL¹] (3), and [NiL²] (4), have been synthesized and characterized by elemental analyses and spectroscopic methods. The crystal structures of these complexes have been determined by X-ray diffraction. The coordination geometry around Cu(II) and Ni(II) centers is described as distorted square planar in all complexes with the CuN₂O₂ coordination more distorted than the Ni ones. The electrochemical studies of these complexes indicate a good correlation between the structural distortion and the redox potentials of the metal centers. The ligand and metal complexes were also screened for their *in vitro* antibacterial activity.

Keywords: Unsymmetrical Schiff base; Copper(II) and nickel(II) complexes; Crystal structure; Cyclic voltammetry; Antibacterial activity

*Corresponding author. Email: amirnasr@cc.iut.ac.ir

1. Introduction

Transition metal-Schiff base complexes have been the subject of extensive investigation due to their biological applications as antibacterial [1–3], antitumor [4–8], and antioxidant [9] agents, and their use in homogeneous or heterogeneous catalysis [10–13]. However, much less attention has been paid to the unsymmetrical Schiff base complexes. Due to the fact that the active sites in most metalloproteins and enzymes are in unsymmetrical environments [14, 15], the unsymmetrical Schiff base complexes clearly offer advantages over their symmetrical counterparts as biological models in understanding the geometry of active sites in the biological systems [15–19]. This class of compounds has also become the focus of attention due to their medical applications [20–22]. In spite of the large number of available antibacterial drugs, new antibiotic resistance has created a substantial medical need for new classes of antibacterial agents. Therefore, significant research is directed towards designing new antibacterial drugs [23–26].

In continuation of our investigation on the synthesis of unsymmetrical Schiff base complexes [27–30], we herein report the synthesis, spectral characterization, crystal structures, electrochemistry, and antibacterial activities of Cu(II) and Ni(II) complexes of the unsymmetrical tetradentate Schiff base ligands, H_2L^1 and H_2L^2 (scheme 1). These ligands have been prepared by condensation of the free amine group of the precursor tridentate ligand Hbacabza [3-(2-aminobenzylimino)-1-phenylbutan-1-ol] [27] with salicylaldehyde and 2-hydroxy-1-naphthaldehyde, respectively. The X-ray crystal structures, electrochemistry, and antibacterial activities of Cu(II) and Ni(II) complexes (**1–4**) are reported and discussed.

2. Experimental

2.1. Materials and general methods

All solvents and chemicals were of commercial reagent grade and used as received from Aldrich and Merck. The precursor tridentate Schiff base, Hbacabza, was prepared as reported [27]. Infrared spectra from KBr pellets were collected on a FT-IR JASCO 680 plus spectrometer from 4000 to 400 cm^{-1} . UV-Vis absorption spectra were recorded on a JASCO V-570 spectrophotometer. 1H -NMR spectra were measured with a BRUKER AVANCE III (400 MHz) spectrometer. Proton chemical shifts are reported in ppm relative to Me_4Si as an internal standard. Elemental analyses were performed using a Perkin-Elmer 2400 II CHNS-O elemental analyzer. Electrochemical properties of these complexes were studied by cyclic voltammetry. Cyclic voltammograms were obtained on a SAMA 500 Research Analyzer using a three-electrode system, a glassy carbon working electrode (Metrohm 6.1204.110 with 2.0 ± 0.1 mm diameter), a platinum disk auxiliary electrode, and an Ag wire as the reference electrode. Cyclic voltammetry measurements were performed in acetonitrile and *N,N*-dimethylformamide (DMF) with tetrabutylammonium hexafluorophosphate as the supporting electrolyte. The solutions were deoxygenated by purging with Ar for 5 min. All electrochemical potentials were calibrated versus internal $Fc^{+/0}$ ($E^0 = 0.40$ V for MeCN and 0.45 V for DMF vs. SCE) couple under the same conditions [31].

2.2. Synthesis

2.2.1. Synthesis of H_2L^1 . A solution of salicylaldehyde (1.22 g, 10 mmol) in ethanol (50 mL) was added to a stirring solution of Hbacabza (2.66 g, 10 mmol) in ethanol (50 mL). The mixture was stirred for 4 h to give a yellow solution. Yellow microcrystalline product was obtained by slow evaporation. The product was filtered off, and washed with cold ethanol, and dried under vacuum. Yield: 75%. Anal. Calcd for $C_{24}H_{22}N_2O_2$: C, 77.81; H, 5.99; N, 7.56. Found: C, 78.62; H, 6.08; N, 7.68%. FT-IR (KBr, cm^{-1}) ν_{max} : 3434 (OH), 1616, 1596 (C=N). UV-Vis: λ_{max} (nm) (ϵ , $M^{-1} cm^{-1}$) (CH_2Cl_2): 281 (13,730), 346 (35,270). λ_{max} (nm) (ϵ , $M^{-1} cm^{-1}$) (DMF): 278 (13,760), 344 (35,340). 1H -NMR ($CDCl_3$, 400 MHz) (δ , ppm): 12.96 (s, 1H, H_a), 11.69 (s, 1H, H_b), 8.62 (s, 1H, H_c), 6.96–7.87 (m, 13H, $H_{aromatic}$), 5.75 (s, 1H, H_d), 4.70–4.71 (d, 2H, H_e), 2.10 (s, 3H, H_f).

2.2.2. Synthesis of H_2L^2 . H_2L^2 was prepared by a procedure similar to that of H_2L^1 except that 2-hydroxy-1-naphthaldehyde (1.72 g, 10 mmol) was used instead of salicylaldehyde. Yield: 40%. Anal. Calcd for $C_{28}H_{24}N_2O_2$: C, 79.98; H, 5.75; N, 6.66. Found: C, 79.62; H, 5.62; N, 6.64%. IR (KBr, cm^{-1}), ν_{max} : 3427 (OH), 1598, 1621 (C=N). UV-Vis: λ_{max} (nm) (ϵ , $M^{-1} cm^{-1}$) (CH_2Cl_2): 275 (17,290), 344 (33,456), 435 (3250), 457 (2470). λ_{max} (nm) (ϵ , $M^{-1} cm^{-1}$) (DMF): 270 (17,310), 344 (33,500), 434 (3265), 456 (2475). 1H -NMR ($CDCl_3$, 400 MHz) (δ , ppm): 15.16 (s, 1H, H_b), 11.53 (s, 1H, H_a), 9.4 (s, 1H, H_c), 7.20–8.2 (m, 15H, $H_{aromatic}$), 5.75 (s, 1H, H_d), 4.46–4.77 (d, 2H, H_e), 2.13 (s, 3H, H_f).

2.2.3. Synthesis of $[CuL^1]$ (1). To a solution of $Cu(OAc)_2 \cdot H_2O$ (19.9 mg, 0.1 mmol) in ethanol (20 mL) was added a solution of H_2L^1 (37.0 mg, 0.1 mmol) in dichloromethane (20 mL) and the mixture was stirred at room temperature for 4 h to give a dark green solution. Green single crystals of **1** suitable for X-ray crystallography were obtained by slow evaporation. The crystals were isolated and washed by cold ethanol and dried under vacuum. Yield 89%. Anal. Calcd for $C_{24}H_{20}CuN_2O_2$: C, 66.73; H, 4.67; N, 6.48. Found: C, 65.39; H, 4.63; N, 6.45%. FT-IR (KBr, cm^{-1}) ν_{max} : 1587, 1613 (C=N). UV-Vis: λ_{max} (nm) (ϵ , $M^{-1} cm^{-1}$) (CH_2Cl_2): 295 (27,330), 353 (19,620), 409(11,110), 610 (256), 716 (40). λ_{max} (nm) (ϵ , $M^{-1} cm^{-1}$) (DMF): 294 (27,295), 356 (19,590), 406 (11,090), 615 (250), 727 (37).

2.2.4. Synthesis of $[CuL^2]$ (2). Complex **2** was prepared by a procedure similar to that of **1** except that H_2L^2 (42.05 mg, 0.1 mmol) in chloroform (20 mL) was used instead of H_2L^1 . Dark green crystals were collected by filtration and washed with small amounts of ethanol. Yield: 70%. Anal. Calcd for $C_{28}H_{22}CuN_2O_2$: C, 69.77; H, 4.60; N, 5.81. Found: C, 70.40; H, 4.50; N, 5.89%. FT-IR (KBr, cm^{-1}) ν_{max} : 1599, 1617 (C=N). UV-Vis λ_{max} (nm) (ϵ , $M^{-1} cm^{-1}$) (CH_2Cl_2): 288 (16,290), 325 (22,070), 335 (22,200), 425 (11,220), 594 (260), 710 (36). λ_{max} (nm) (ϵ , $M^{-1} cm^{-1}$) (DMF): 288 (16,235), 323 (22,005), 356 (22,135), 427 (11,185), 599 (260), 720 (28).

2.2.5. Synthesis of $[NiL^1]$ (3). Complex **3** was prepared by a procedure similar to that of **1** except that $Ni(OAc)_2 \cdot 4H_2O$ salt (24.8 mg, 0.1 mmol) was used instead of $Cu(OAc)_2 \cdot H_2O$. The resulting dark brown crystals were filtered off, washed with cold ethanol, and dried

under vacuum. Yield 68%. Anal. Calcd for $C_{24}H_{20}NiN_2O_2$: C, 67.49; H, 4.72; N, 6.56. Found: C, 65.80; H, 4.54; N, 6.51%. FT-IR (KBr, cm^{-1}) ν_{max} : 1592, 1611 (C=N). UV-Vis: λ_{max} (nm) (ϵ , $M^{-1} cm^{-1}$) (CH_2Cl_2): 291 (25,160), 346 (11,270), 404 (6050), 453 (6300), 480 (3320), 618 (150). λ_{max} (nm) (ϵ , $M^{-1} cm^{-1}$) (DMF): 291 (25,125), 343 (11,250), 408 (6045), 451 (6295), 486 (3310), 616 (148).

2.2.6. Synthesis of $[NiL^2]$ (4). Complex **4** was prepared by a procedure similar to that of **2** except that $Ni(OAc)_2 \cdot 4H_2O$ salt (24.8 mg, 0.1 mmol) was used instead of $Cu(OAc)_2 \cdot H_2O$. The resulting brown crystals were collected by filtration and washed with small amounts of ethanol. Yield: 90%. Anal. Calcd for $C_{28}H_{22}NiN_2O_2$: C, 70.48; H, 4.65; N, 5.87. Found: C, 70.47; H, 4.50; N, 5.89%. FT-IR (KBr, cm^{-1}), ν_{max} : 1597, 1616 (C=N). UV-Vis λ_{max} (nm) (ϵ , $M^{-1} cm^{-1}$) (CH_2Cl_2): 288 (21,170), 314 (21,020), 319 (21,960), 362 (12,480), 396 (7050), 450 (6610), 482 (3725), 606 (210). λ_{max} (nm) (ϵ , $M^{-1} cm^{-1}$) (DMF): 286 (21,205), 324 (21,055), 362 (12,500), 453 (7060), 487 (3730), 604 (212).

2.3. Crystal structure determination

Suitable single crystals of the complexes were obtained by slow evaporation of an ethanol–dichloromethane (1 : 1 v/v) solution of **1**, a chloroform–ethanol (1 : 1 v/v) solution of **2** and **4**, and an ethanol solution of **3** at room temperature. X-ray data of **1–4** were collected at $T = 100$ K on a Bruker Kappa APEX-II CCD diffractometer with graphite-monochromated

Table 1. Crystallographic parameters, data collection, and refinement details for $[CuL^1]$ (**1**), $[CuL^2]$ (**2**), $[NiL^1]$ (**3**), and $[NiL^2]$ (**4**).

Compound	1	2	3	4
Empirical formula	$C_{24}H_{20}CuN_2O_2$	$C_{28}H_{22}CuN_2O_2$	$C_{24}H_{20}NiN_2O_2$	$C_{28}H_{22}NiN_2O_2$
Formula weight	431.96	482.02	427.13	477.19
Temperature (K)	100(2)	100(2)	100(2)	100(2)
Crystal system	Orthorhombic	Orthorhombic	Orthorhombic	Orthorhombic
Space group	$P2_12_12_1$	$Pbca$	$Pbca$	$Pbca$
a (Å)	7.1509(10)	17.3807(3)	11.2421(2)	17.8071(3)
b (Å)	12.0589(2)	12.8608(3)	12.8952(3)	12.2237(3)
c (Å)	21.8025(3)	18.9271(4)	26.3710(5)	19.4703(4)
V (Å ³)	1880.07(5)	4230.77(15)	3822.98(13)	4238.07(12)
Z	4	8	8	8
D_{calc} ($Mg m^{-3}$)	1.526	1.513	1.484	1.496
μ (mm^{-1})	1.186	1.063	1.038	0.946
Crystal size (mm)	$0.58 \times 0.20 \times 0.05$	$0.52 \times 0.22 \times 0.18$	$0.55 \times 0.50 \times 0.46$	$0.56 \times 0.28 \times 0.26$
$F(000)$	892	1992	1776	1984
θ range (°)	1.87–30.0	2.15–30.0	2.38–29.98	2.09–30.00
Absorption correction	Multi-scan	Multi-scan	Multi-scan	Multi-scan
Reflections collected	22,506	101,971	25,983	74,479
R_{int}	0.0335	0.0479	0.0203	0.0324
Data/restraints/ parameters	5467/0/263	6154/0/299	5545/0/264	6167/0/299
Goodness-of-fit on F^2	1.075	1.032	1.049	1.072
Final R indices	$R_1 = 0.0308$, $wR_2 = 0.0702$	$R_1 = 0.0302$, $wR_2 = 0.0780$	$R_1 = 0.0364$, $wR_2 = 0.0908$	$R_1 = 0.0306$, $wR_2 = 0.0837$
Largest diff. peak / hole ($e \text{ \AA}^{-3}$)	0.64/−0.22	0.49/−0.54	0.82/−0.21	0.48/−0.48

^a $R_1 = \sum |F_o| - |F_c| / \sum |F_o|$, $wR_2 = \{ \sum [w(F_o^2 - F_c^2)]^2 / \sum [w(F_o^2)]^2 \}^{1/2}$.

Mo $K\alpha$ ($\lambda = 0.71073 \text{ \AA}$) radiation. Cell refinement was performed with SAINT, and data reduction with the program SAINT [32]. Correction for absorption was carried out with the multi-scan method and program SADABS [32]. The structures of these complexes were solved with direct methods using SHELXS97 [33] and structure refinement on F^2 was carried out with SHELXL97. Crystal data together with other relevant information on the structure determination are summarized in table 1.

2.4. Antibacterial activity

The antibacterial activities of H_2L^1 , H_2L^2 , and **1–4** were tested by the well-known diffusion method using Sabouraud dextrose agar and Müller Hinton agar [34]. The zone of inhibition was recorded on completion of the incubation as the mean diameter for each complex at 100–500 $\mu\text{g mL}^{-1}$ concentrations. Stock solutions of ligands and **1–4** were prepared in dimethyl sulfoxide (DMSO). The diameters of the minimum zone of inhibition (MZI) produced by the compounds were compared with the standard antibiotic penicillin of 100–500 $\mu\text{g mL}^{-1}$ concentrations. Each test was carried out three times to minimize the error. In order to clarify any effect of DMSO in the biological screening, blank studies were carried out and no activity was observed against any bacterial strains in pure DMSO.

Minimum inhibitory concentration (MIC) is the lowest concentration of an antimicrobial compound that will inhibit the visible growth of micro-organisms at 37 °C after overnight incubation. MICs are important in diagnostic laboratories to confirm the resistance of micro-organisms to antimicrobial agents and also to monitor the activity of new antimicrobial agents. The MIC of the ligands and the corresponding Cu(II) and Ni(II) complexes was tested against bacterial strains through the broth dilution method. In this method, the test concentrations of compounds were made from 50 to 400 $\mu\text{g mL}^{-1}$ in sterile wells. The MIC was determined by reading each well at 600 nm with a spectrophotometer before and after overnight incubation for the determination of transparency ($T\%$).

3. Results and discussion

3.1. Synthesis and characterization

The tetradentate Schiff bases, H_2L^1 or H_2L^2 , were prepared by condensation of the free amino group of the precursor tridentate ligand, Hbacabza, with salicylaldehyde and 2-hydroxy-1-naphthaldehyde, respectively. The nickel and copper complexes (scheme 2) were synthesized by the direct reaction of the corresponding ligand, H_2L^1 or H_2L^2 , with the corresponding metal acetate at room temperature. Crystals of these complexes suitable for X-ray crystallography were obtained in good yield (70–90%). L^1 and L^2 are dianionic tetradentate ligands and coordinate in their doubly deprotonated form forming three six-membered chelate rings surrounding the central metal ions.

3.2. Description of structures

3.2.1. Crystal structure of $[CuL^1]$ (1) and $[CuL^2]$ (2). The crystal structures of $[CuL^1]$ and $[CuL^2]$ with atomic numbering scheme are presented in figures 1 and 2, respectively,

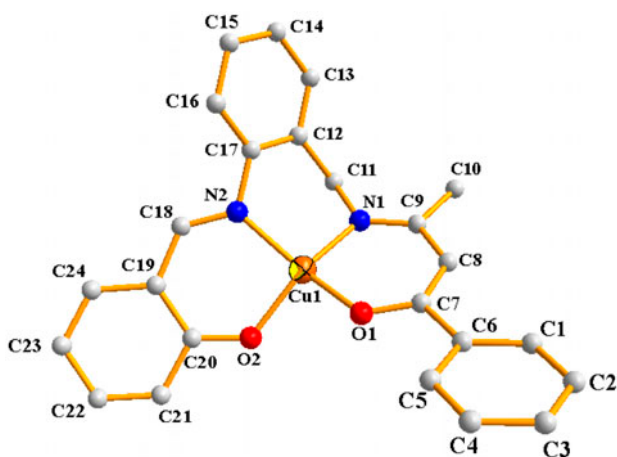


Figure 1. The molecular structure of $[\text{CuL}^1]$ (**1**) with its atom labeling.

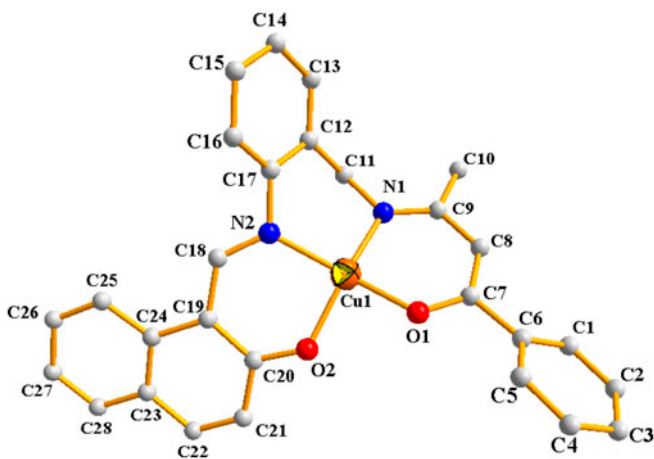
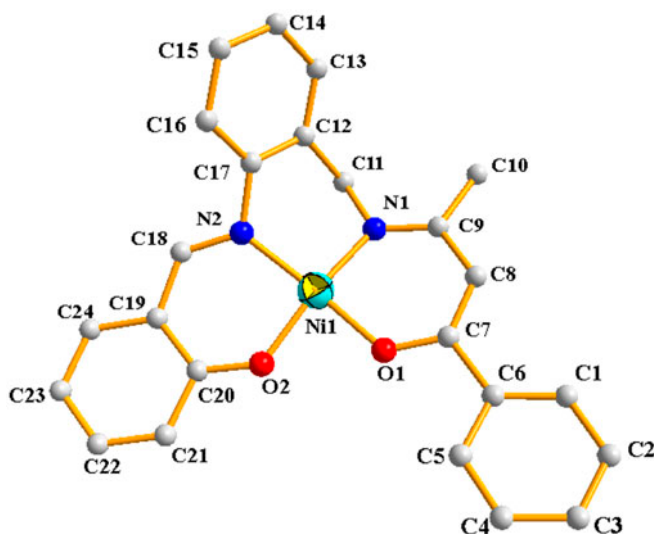


Figure 2. The molecular structure of $[\text{CuL}^2]$ (**2**) with its atom labeling.

and the selected bond distances and angles are listed in table 2. The complexes crystallize in the orthorhombic crystal system, space group $P2_12_12_1$ for **1**, and $Pbca$ for **2**. The Schiff bases are tetradentate-chelating ligands that are coordinated with Cu(II). The O–Cu–N *trans* angles are in 148.6 – 159.8° range, indicating that the coordination geometry around copper is a strongly distorted-puckered square. The observed distortion of the CuN_2O_2 coordination is mainly due to the rigid phenylmethylidene group bridging the two imine nitrogens, in contrast to a flexible 1,3-alkylidene bridge for instance. In case of **1**, the distortion appears to be enhanced by packing effects. The dihedral angles between the two N,O-chelate rings ($\text{Cu1-N1-C9-C8-C7-O1-}$ and $\text{Cu1-N2-C18-C19-C20-O2-}$) are 40.41° and 28.35° in **1** and **2**, respectively. The average bond lengths $\text{Cu-O} = 1.907 \text{ \AA}$ and $\text{Cu-N} = 1.953 \text{ \AA}$ are comparable to those observed in Cu(II) Schiff base complexes with identical coordination

Table 2. Selected bond lengths (Å) and angles (°) for **1–4**.

	1	2	3	4
<i>Bond lengths</i>		<i>Bond lengths</i>		
Cu1–O1	1.9079(13)	1.8940(11)	Ni1–O1	1.8498(10)
Cu1–O2	1.9101(13)	1.9166(11)	Ni1–O2	1.8544(10)
Cu1–N1	1.9321(16)	1.9443(13)	Ni1–N1	1.8822(12)
Cu1–N2	1.9738(15)	1.9599(13)	Ni1–N2	1.9013(12)
<i>Bond angles</i>		<i>Bond angles</i>		
O1–Cu1–O2	90.50(6)	86.80(5)	O1–Ni1–O2	82.12(5)
O1–Cu1–N1	94.61(6)	94.87(5)	O1–Ni1–N1	92.90(5)
O1–Cu1–N2	148.67(6)	159.85(5)	O1–Ni1–N2	169.81(5)
O2–Cu1–N1	152.52(7)	158.29(5)	O2–Ni1–N1	169.37(5)
O2–Cu1–N2	94.20(6)	90.85(5)	O2–Ni1–N2	92.72(5)
N1–Cu1–N2	95.30(7)	94.66(5)	N2–Ni1–N1	93.57(5)


 Figure 3. The molecular structure of $[NiL^1]$ (**3**) with its atom labeling.

spheres [29, 35]. A sample of 37 comparable Cu complexes taken from the CCDC database [36] gave mean values of Cu–O = 1.906(21) Å and Cu–N = 1.959(24) Å.

3.2.2. Crystal structure of $[NiL^1]$ (3**) and $[NiL^2]$ (**4**).** The crystal structures of $[NiL^1]$ and $[NiL^2]$ with atomic numbering scheme are presented in figures 3 and 4, respectively, and selected bond distances and angles are listed in table 2. Both complexes crystallize in the orthorhombic crystal system and space group $Pbca$. The Schiff bases are tetradentate-chelating ligands. The central Ni(II) ions have a modestly distorted square planar geometry. The *trans* angles N1–Ni–O2 and N2–Ni–O1 are 164.4–169.8°. The dihedral angles between the two N,O-chelate rings are 11.98° and 19.97° in **3** and **4**, respectively. The average Ni–O and Ni–N bond lengths are 1.854 and 1.888 Å and agree well with the corresponding distances in related Ni(II) complexes [29, 37].

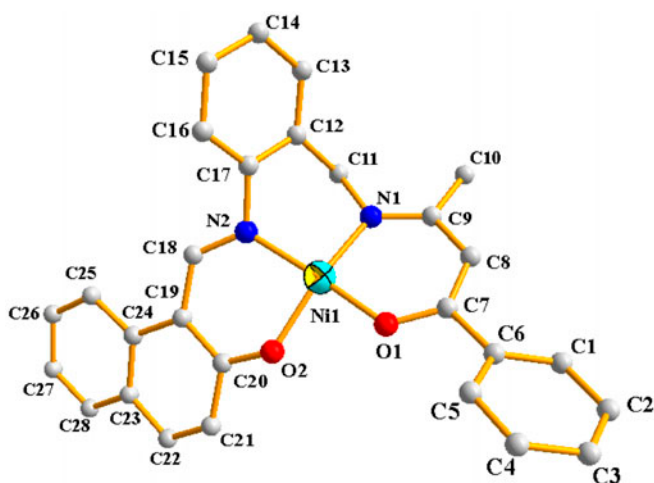


Figure 4. The molecular structure of $[\text{NiL}^2]$ (4) with its atom labeling.

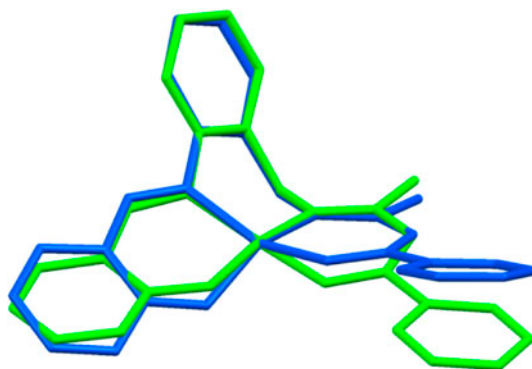


Figure 5. Comparison of the molecular structure of $[\text{CuL}^1]$ (blue) and $[\text{NiL}^1]$ (green) (see <http://dx.doi.org/10.1080/00958972.2015.1085977> for color version).

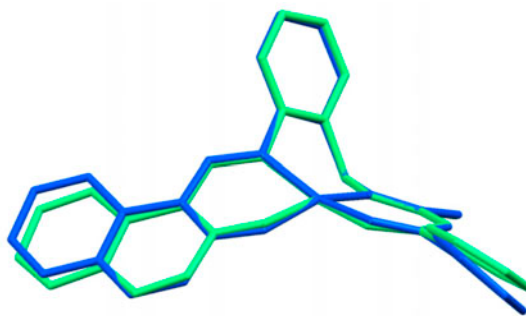


Figure 6. Comparison of the molecular structure of $[\text{CuL}^2]$ (blue) and $[\text{NiL}^2]$ (green) (see <http://dx.doi.org/10.1080/00958972.2015.1085977> for color version).

The difference in mean bond lengths (such as Cu–O,N of **1** minus Ni–O,N of **3** = 0.059 Å) corresponds approximately to the difference in standard ionic radii and the presence of electron in the $d_{x^2-y^2}$ orbital in the Cu(II) complexes. Note that the Cu coordination geometry is more distorted than that of the analogous NiL^1 complex as shown in figure 5 (see also *trans*-bond angles).

A comparison between the isostructural complexes $[NiL^2]$ (**4**) and $[CuL^2]$ (**2**) (figure 6) shows that the NiO_2N_2 fragment is less distorted than the CuO_2N_2 fragment (see also *trans*-bond angles), but reveals that the two terminal phenyl rings exhibit larger differences in orientation.

3.3. Spectral characterization

The FT-IR spectral data of H_2L^1 , H_2L^2 and **1–4** are presented in the supplementary material. The absence of $\nu(OH)$ in spectra of the metal(II) Schiff base complexes confirms the involvement of phenolate O in chelation. The characteristic bands of two different imine (C=N) groups in the free unsymmetrical Schiff bases, 1596 and 1616 cm^{-1} for H_2L^1 , and 1598 and 1621 cm^{-1} for H_2L^2 are shifted to lower wave numbers in the spectra of **1–4** at 1587–1617 cm^{-1} , indicating that nitrogen of the azomethine is coordinated.

The electronic absorption spectra of H_2L^1 , H_2L^2 and **1–4** are recorded in CH_2Cl_2 and DMF solutions and the data are presented in the supplementary material. The absorption spectra of free ligands consist of intense bands from 270 to 455 nm and are attributed to intraligand ($n \rightarrow \pi^*$ and $\pi \rightarrow \pi^*$) and charge-transfer transitions. These spectral features are also present in the spectra of their metal complexes. The spectra of Cu(II) complexes in CH_2Cl_2 solution show a shoulder at 716 nm and an absorption band at 610 nm for $[CuL^1]$ (**1**) and 710 and 594 nm for $[CuL^2]$ (**2**), respectively, assigned to the ${}^2B_{1g} \rightarrow {}^2A_{1g}$ and ${}^2B_{1g} \rightarrow {}^2E_g$ transitions of square planar geometry [38]. These transitions are at 727 and 615 nm for **1**, and 720 and 599 nm for **2** in DMF solution and can also be attributed to ${}^2B_1 \rightarrow {}^2A_1$ and ${}^2B_1 \rightarrow {}^2E$ transitions [38]. The blue shift in the position of the ligand-field transitions in $[CuL^2]$ relative to the $[CuL^1]$ is due to the higher ligand field strength of L^2 as compared to that of L^1 , originating from a better overlap between the Cu(II) $d_{x^2-y^2}$ orbital and the O–N donors of the less-distorted L^2 ligand. The Cu(II) complexes show relatively intense bands in the 288–425 nm region corresponding to the intraligand and charge-transfer transitions.

The Ni(II) complexes (**3** and **4**) show a band at 618 nm in CH_2Cl_2 (616 nm in DMF) for $[NiL^1]$ (**3**) and 606 nm in CH_2Cl_2 (604 nm in DMF) for $[NiL^2]$ (**4**), assigned to ${}^1A_{1g} \rightarrow {}^1E_g$ transition, and are consistent with the low-spin square planar geometry [38]. In addition, a shoulder is observed at 480 nm. In view of its relatively large intensity, it is probably the second ligand field transition mixed with charge-transfer character. The higher energy ligand field bands are probably covered by the more intense charge-transfer bands. The relatively intense bands from 288 to 453 nm are due to the intraligand and charge-transfer transitions.

The 1H -NMR spectral measurements of H_2L^1 and H_2L^2 were performed in $CDCl_3$ solution and the corresponding data are given in the Supplementary Material. The main features of the 1H -NMR spectra of the unsymmetrical Schiff base ligands are the signals due to two different phenolic groups at 12.96 and 11.69 ppm for H_2L^1 , and 15.15 and 11.53 ppm for H_2L^2 . The CH_{imine} signal is at 8.50 ppm for H_2L^1 and at 9.4 ppm for H_2L^2 . The signal of

Table 3. Redox potential data of 1–4 in MeCN and DMF.

Solvent	MeCN			DMF			Dihedral angle (°)
	$E_{pc}(II \rightarrow I)$ (V)	$E_{pa}(I \rightarrow II)$ (V)	ΔE (mV)	$E_{pc}(II \rightarrow I)$ (V)	$E_{pa}(I \rightarrow II)$ (V)	ΔE (mV)	
[CuL ¹] (1)	-1.125	-1.048	77	-1.157	-1.012	145	40.42
[CuL ²] (2)	-1.090	-1.015	75	-1.151	-1.070	81	28.35
[NiL ¹] (3)	-1.499	-1.430	69	-1.504	-1.412	92	11.98
[NiL ²] (4)	-1.523	-1.458	65	-1.514	-1.438	76	19.97

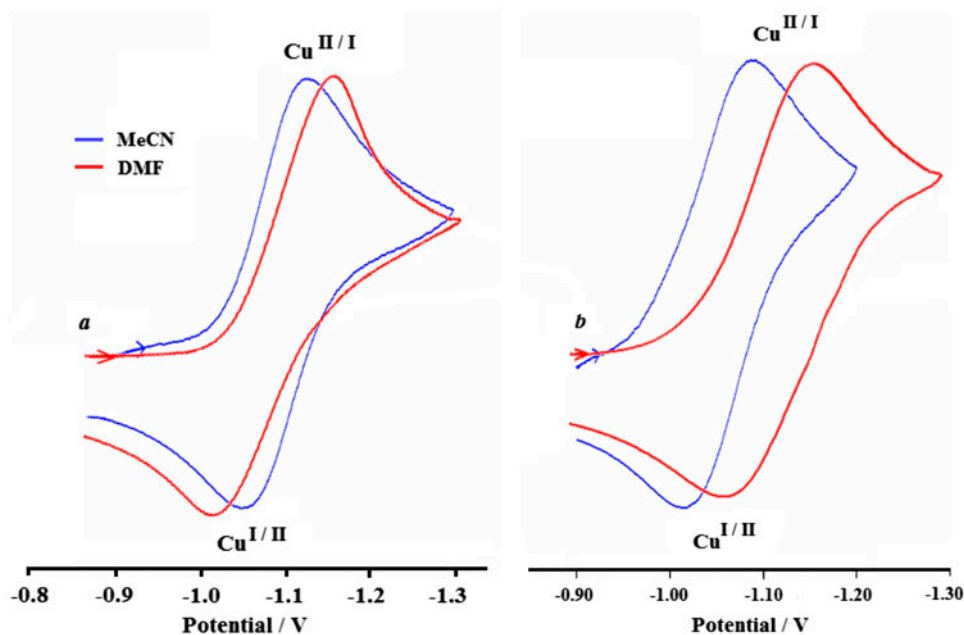


Figure 7. Cyclic voltammograms of (a) [CuL¹] and (b) [CuL²] in MeCN and DMF at 298 K, $C \approx 10^{-3}$ M, and scan rate = 100 mV s⁻¹.

CH₃ substituent appears at 2.10 and 2.13 ppm for H₂L¹ and H₂L², respectively. The aromatic protons of these compounds are from 5.7 to 8.2 ppm.

3.4. Electrochemical studies

The electrochemical properties of Cu(II) and Ni(II) complexes were investigated in acetonitrile and DMF, and the electrochemical data are summarized in table 3. The cyclic voltammograms of the Cu(II) complexes are shown in figure 7. A nearly reversible Cu^{II/I} reduction process is observed at -1.125 V ($\Delta E = 77$ mV) for [CuL¹] and at -1.090 V ($\Delta E = 75$ mV) for [CuL²] in acetonitrile solution. The reduction potential of [CuL¹] is slightly more negative (35 mV) than that of [CuL²]. This difference may arise from the difference in the extent of structural distortion in the two complexes. Considering the dihedral

angle of 40.42° between the two chelating rings in $[CuL^1]$ and 28.35° in $[CuL^2]$, less-efficient π -backbonding is expected for the more distorted $[CuL^1]$. This in turn leads to a higher electron density on copper in $[CuL^1]$ and, as a result, its reduction at a more negative potential relative to $[CuL^2]$. In DMF solution, a quasi-reversible $Cu(II)$ – $Cu(I)$ reduction process ($\Delta E = 145$ mV) at -1.157 V for the $[CuL^1]$ and at -1.151 V ($\Delta E = 81$ mV) $[CuL^2]$ is observed. These data indicate that the $Cu(II)$ – $Cu(I)$ reduction is less reversible in DMF as compared to CH_3CN . A possible explanation for this feature is that the $Cu(II)$ complexes are partially coordinated by solvent molecules in DMF solution. This is evident from the more negative reduction potentials of these complexes in DMF (-1.157 and -1.151 V) relative to those observed in acetonitrile (-1.125 and -1.090 V). In addition, L^1 has a tendency to be distorted towards tetrahedral while chelating to a d^9 $[Cu(II)]$ or $Ni(I)$ or a d^{10} $[Cu(I)]$ metal ion, but L^2 containing a naphthalene ring maintains more planar configuration, where the structural change for $M(II)/M(I)$ is very small in going from MeCN to DMF.

The cyclic voltammograms for $Ni(II)$ complexes in DMF and acetonitrile are shown in figure 8. In acetonitrile solution, the $[NiL^1]$ and $[NiL^2]$ complexes exhibit a reversible $Ni^{II/I}$ reduction process at -1.499 and -1.523 V, respectively. In this case, the reduction potential in the more distorted $[NiL^2]$ is more negative than that of $[NiL^1]$. The dihedral angles between the two chelating rings are 19.97° and 11.98° for $[NiL^2]$, and $[NiL^1]$, respectively, and as expected, the reduction wave appears at a more negative potential for $[NiL^2]$ relative to $[NiL^1]$. Contrary to the copper complexes, the electrochemical behavior of the two nickel complexes in DMF solution is not changed appreciably as compared to that observed in acetonitrile solution. A quasi-reversible $Ni^{II/I}$ reduction process at -1.504 V ($\Delta E = 92$ mV) is observed for $[NiL^1]$ and a nearly reversible reduction process at -1.514 V ($\Delta E = 76$ mV) for $[NiL^2]$. This is presumably due to the fact that the nickel complexes avoid any noticeable structural transformation in going from MeCN to DMF. However, as in the case of copper complexes, the tendency of L^2 in keeping a planar configuration may contribute to the reversibility observed in $[NiL^2]$ reduction as compared to $[NiL^1]$.

The reduction process of $Ni(II)$ complexes occurs at a more negative potential relative to copper analogs. This is presumably due to the fact that d^8 is the most favorable electronic

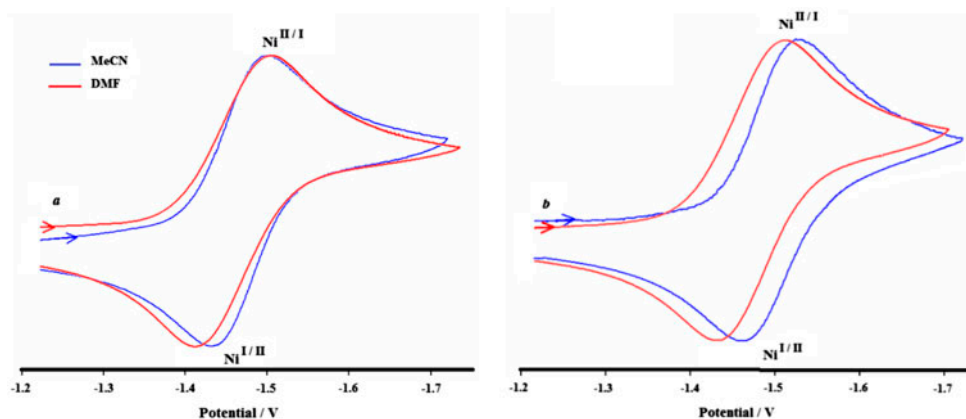
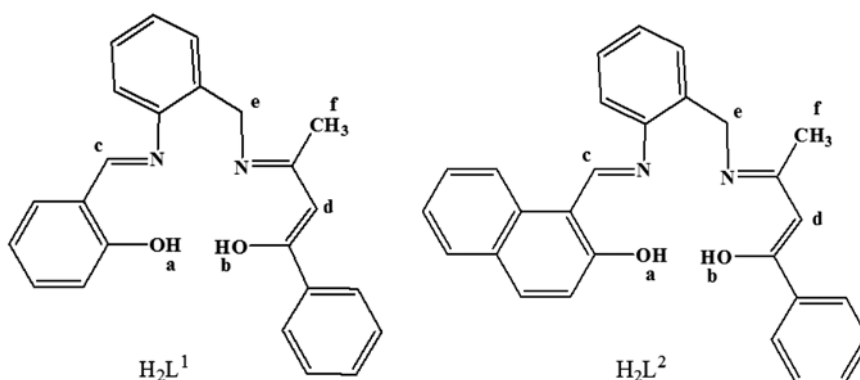
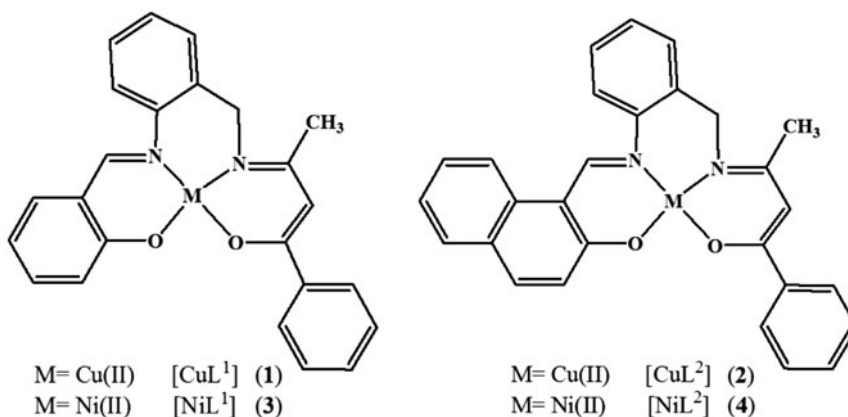


Figure 8. Cyclic voltammograms of (a) $[NiL^1]$ and (b) $[NiL^2]$ in MeCN and DMF at 298 K, $C \approx 10^{-3}$ M, and scan rate = 100 mV s^{-1} .



Scheme 1. The syntax formula of the Schiff base ligands, H_2L^1 and H_2L^2 .



Scheme 2. The syntax formula of the Schiff base complexes (1–4).

configuration for the square planar transition metal complexes and deviation from that leads to some instabilities in planar complexes of the tetradentate Schiff base ligands [39].

3.5. Antibacterial activity

The ligands and their corresponding metal complexes were tested for antibacterial activity against *Bacillus cereus* and *Staphylococcus aureus* as Gram +ve, and *Klebsiella pneumoniae* and *Escherichia coli* as Gram –ve species. The MIC values are in the range 300–400 $\mu\text{g mL}^{-1}$ against *B. cereus* (H_2L^1 , 300 $\mu\text{g mL}^{-1}$; H_2L^2 , 300 $\mu\text{g mL}^{-1}$; **1**, 300 $\mu\text{g mL}^{-1}$; **2**, 350 $\mu\text{g mL}^{-1}$; **3**, 400 $\mu\text{g mL}^{-1}$; **4**, 350 $\mu\text{g mL}^{-1}$). The screening results (MZI) are summarized in table 4. The data indicate that the antibacterial activity of the ligands and their metal complexes is the highest against *B. cereus* among all the bacteria tested. For example, all compounds at 400 $\mu\text{g mL}^{-1}$ concentration exhibit antibacterial activity against *B. cereus* [H_2L^1 (MZI = 34 mm), H_2L^2 (MZI = 35 mm), **1** (MZI = 30 mm), **2** (MZI = 32 mm), **3** (MZI = 25 mm), and **4** (MZI = 32 mm)], comparable to that observed for penicillin (MZI = 40 mm). Moreover, the antibacterial effect of these compounds on *B. cereus* is more

Table 4. Minimum zone of inhibition (MZI, in mm) for the antimicrobial activity of H_2L^1 , H_2L^2 , **1**, **2**, **3**, and **4**.

Compound	Conc. ($\mu\text{g mL}^{-1}$)	<i>B. cereus</i>	<i>S. aureus</i>	<i>K. pneumoniae</i>	<i>E. coli</i>
H_2L^1	500	38	22	15	16
	400	34	16	10	13
	300	22	14	9	11
	200	16	12	8	10
	100	13	9	7	None
H_2L^2	500	39	28	12	17
	400	35	25	8	14
	300	22	20	7	13
	200	15	15	None	11
	100	11	10	None	9
[CuL ¹]	500	34	11	12	14
	400	30	None	10	12
	300	20	None	9	11
	200	13	None	8	10
	100	10	None	None	8
[CuL ²]	500	35	12	11	14
	400	32	None	10	12
	300	20	None	8	11
	200	14	None	7	10
	100	12	None	None	8
[NiL ¹]	500	29	13	11	15
	400	25	8	9	10
	300	18	7	8	9
	200	16	None	7	7
	100	13	None	None	None
[NiL ²]	500	36	15	12	14
	400	32	10	8	10
	300	21	9	7	8
	200	13	8	None	7
	100	9	None	None	None
Penicillin	500	65	55	15	25
	400	40	50	12	22
	300	38	44	11	21
	200	35	40	10	19
	100	28	32	8	17
DMSO		None	None	None	None

than that reported for related compounds, [CuL]²⁻ (MZI = 15 mm) [L = bis(indoline-2-one) triethylenetetramine] [20], [CuL¹]²⁻ (MZI = 19 mm), [NiL¹]²⁻ (MZI = 12 mm), and [NiL²]²⁻ (MZI = 14 mm) [L¹ = (E)-7-methoxy-N1-(2,4,5-trimethoxybenzylidene)benzofuran-2-carbohydrazide, L² = (E)-N1-(2,6-dichlorobenzylidene)-7-methoxybenzofuran-2-carbohydrazide] [21].

4. Conclusion

In this investigation, we have reported the synthesis and characterization of two unsymmetrical N_2O_2 Schiff base ligands (H_2L^1 and H_2L^2) and their Cu(II) and Ni(II) complexes. The crystal structures of these complexes have been determined by X-ray

crystallography. The coordination around Cu(II) and Ni(II) centers is distorted-puckered squares in all complexes, which is mainly due to the presence of the rigid $-\text{C}_{\text{phenyl}}-\text{C}_{\text{phenyl}}-\text{CH}_2$ -spacer between the two nitrogens of the ligands. The puckering of the CuO_2N_2 coordination is bigger than that of their NiO_2N_2 pendants which appears to be attributable to electronic effects (d^9 vs. low-spin d^8 configuration) and to the difference in standard ionic radii of Cu^{II} and Ni^{II} . The cyclic voltammetry studies (in MeCN) show good agreement between the structural distortion and the redox potentials of the metal centers. The ligand and metal complexes were screened for their *in vitro* antimicrobial activity. Antimicrobial tests showed that the synthesized compounds possess biological activities and are effective on *B. cereus*. However, the exact mechanism is unrevealed and further biological studies are necessary to get a clear picture of this behavior.

Supplementary material

CCDC numbers 847675–847678 contain the supplementary crystallographic data for complexes **1**, **3**, **4**, and **2**, respectively. These data can be obtained free of charge from the Cambridge Crystallographic Data Center via www.ccdc.cam.ac.uk/data_request/cif.

Acknowledgements

Partial support of this work by the Isfahan University of Technology Research Council is gratefully acknowledged. The X-ray center of the Vienna University of Technology is acknowledged for providing access to the single-crystal diffractometer.

Disclosure statement

No potential conflict of interest was reported by the authors.

Supplemental data

Supplemental data for this article can be accessed at <http://dx.doi.org/10.1080/00958972.2015.1085977>

References

- [1] K. Vashi, H.B. Naik. *Eur. J. Chem.*, **1**, 272 (2004).
- [2] A.K. Bhendkar, K. Vijay, A.W. Raut. *Acta Ciencia Indica Chem.*, **30**, 29 (2004).
- [3] M. Patil, R. Hunoor, K. Gudasi. *Eur. J. Med. Chem.*, **45**, 2981 (2010).
- [4] N.A. Negm, M.F. Zaki. *Colloids Surf. B: Biointerfaces*, **64**, 179 (2008).
- [5] V.P. Daniel, B. Murukan, B.S. Kumari, K. Mohanan. *Spectrochim. Acta, Part A*, **70**, 403 (2008).
- [6] P.K. Sasmal, R. Majumdar, R.R. Dighe, A.R. Chakravarty. *Dalton Trans.*, **39**, 7104 (2010).
- [7] B.S. Creaven, E. Czeglédi, M. Devereux, E.A. Enyedy, A. Foltyn-Arfa Kia, D. Karcz, A. Kellett, S. McClean, N.V. Nagy, A. Noble, A. Rockenbauer, T. Szabó-Plánka, M. Walsh. *Dalton Trans.*, **39**, 10854 (2010).
- [8] X. Qiao, Z.-Y. Ma, C.-Z. Xie, F. Xue, Y.-W. Zhang, J.-Y. Xu, Z.-Y. Qiang, J.-S. Lou, G.-J. Chen, S.-P. Yan. *J. Inorg. Biochem.*, **105**, 728 (2011).

- [9] Z.-C. Liu, B.-D. Wang, Z.-Y. Yang, Y. Li, D.-D. Qin, T.-R. Li. *Eur. J. Med. Chem.*, **44**, 4477 (2009).
- [10] M. Itagaki, K. Hagiya, M. Kamitamari, K. Masumoto, K. Suenobu, Y. Yamamoto. *Tetrahedron*, **60**, 7835 (2004).
- [11] L.D. Pinto, J. Dupont, R.F. de Souza, K. Bernardo-Gusmão. *Catal. Commun.*, **9**, 135 (2008).
- [12] X. Jia, L. Yin, X. Zhao, X.S. Li. *Chin. Chem. Lett.*, **18**, 275 (2007).
- [13] G. Lai, S. Wang, Z. Wang. *Tetrahedron: Asymmetry*, **19**, 1813 (2008).
- [14] E. Kwiatkowski, M. Kwiatkowski. *J. Chem. Soc., Dalton Trans.*, 803 (1985).
- [15] R. Atkins, G. Brewer, E. Kokot, G.M. Mockler, E. Sinn. *Inorg. Chem.*, **24**, 127 (1985).
- [16] A.A. Khandar, S.A. Hosseini-Yazdi, S.A. Zarei. *Inorg. Chim. Acta*, **358**, 3211 (2005).
- [17] P.K. Mascharak. *Coord. Chem. Rev.*, **225**, 201 (2002).
- [18] A.S. Al-Shihri. *Spectrochim. Acta, Part A*, **60**, 1189 (2004).
- [19] R.C. Elder, E.A. Blubaugh Jr., W.R. Heinmann, P.J. Bruke, R.D. McMillian. *Inorg. Chem.*, **22**, 2771 (1983).
- [20] S.I. Al-Resayes, M. Shakir, A. Abbasi, K.M.Y. Amin, A. Lateef. *Spectrochim. Acta, Part A*, **93**, 86 (2012).
- [21] N.S. Reddy, B.S. Shankara, P.M. Krishana, C. Basavaraj, B. Mahesh. *Int. J. Inorg. Chem.*, **2013**, 1 (2013).
- [22] B. Rizwana, S. Santha Lakshmi. *Int. J. Chem. Tech. Res.*, **4**, 464 (2012).
- [23] R.S. Joseyphus, M.S. Nair. *Mycobiology*, **36**, 93 (2008).
- [24] K. Shanker, R. Rohini, V. Ravinder, P.M. Reddy, Y.-P. Ho. *Spectrochim. Acta, Part A*, **73**, 205 (2009).
- [25] R. Sahu, D.S. Thakur, P. Kashyap. *Int. J. Pharm. Sci. Nanotech.*, **5**, 1757 (2012).
- [26] M.L. Low, L. Maigre, P. Dorlet, R. Guillot, J.M. Pagès, K.A. Crouse, C. Policar, N. Delsuc. *Bioconjugate Chem.*, **25**, 2269 (2014).
- [27] S. Meghdadi, K. Mereiter, V. Langer, A. Amiri, R. Erami, A.A. Massoud, M. Amirasr. *Inorg. Chim. Acta*, **385**, 31 (2012).
- [28] S. Meghdadi, M. Amirasr, K. Mereiter, H. Molaei, A. Amiri. *Polyhedron*, **30**, 1651 (2011).
- [29] S. Meghdadi, M. Amirasr, M. Bagheri, F. Najafabadi, K. Mereiter, K.J. Schenk, F. Ziaee. *J. Iran Chem. Soc.*, **11**, 985 (2014).
- [30] M. Amirasr, M. Bagheri, K. Mereiter. *C. R. Chimie*, **16**, 1091 (2013).
- [31] N.G. Connelly, W.E. Geiger. *Chem. Rev.*, **96**, 877 (1996).
- [32] Bruker Programs APEX2, SAINT, XPREP and SADABS. Bruker AXS Inc., Madison, Wisconsin, USA (2008).
- [33] G.M. Sheldrick. *Acta Cryst. A*, **64**, 112 (2008).
- [34] S. Magaldi, S. Mata-Essayag, C. Hartung de Capriles, C. Perez, M.T. Colella, C. Olaiola, Y. Ontiveros. *Int. J. Infect. Dis.*, **8**, 39 (2004).
- [35] S. Chattopadhyay, M.S. Ray, S. Chaudhuri, G. Mukhopadhyay, G. Bocelli, A. Cantoni, A. Ghosh. *Inorg. Chim. Acta*, **359**, 1367 (2006).
- [36] F.R. Allen. *Acta Cryst. B*, **58**, 380 (2002).
- [37] M. Lashanizadegan, M. Jamshidbeigi. *J. Sci. I. R. Iran*, **22**, 121 (2011).
- [38] A.B.P.Lever, *Inorganic Electronic Spectroscopy*, 2nd Edn, p. 535, 565, Elsevier, Amsterdam (1984).
- [39] A. Anthonyamy, S. Balasubramanian. *Inorg. Chem. Commun.*, **8**, 908 (2005).